Polymer vs Solvent Diagram of Film Structures Formed in Spin-Cast Poly(3-alkylthiophene) Blends

J. Jaczewska,[§] A. Budkowski,*[,§] A. Bernasik,[†] E. Moons,[‡] and J. Rysz[§]

M. Smoluchowski Institute of Physics, Jagiellonian University, Reymonta 4, 30-059 Kraków, Poland, Faculty of Physics and Applied Computer Science, AGH-University of Science and Technology, Al. Mickiewicza 30, 30-059 Krakow, Poland, and Department of Physics, Karlstad University, SE-651 88 Karlstad, Sweden

Received October 16, 2007; Revised Manuscript Received February 11, 2008

ABSTRACT: A polymer vs solvent diagram of film structures, formed in polystyrene (PS) blends (1:1 w:w PS/PT) with poly(3-alkylthiophenes) PT [regioregular R-P3DDT, R-P3HT and regiorandom P3BT, P3DDT] spin-coated onto oxidized silicon surfaces from various common solvents [*p*-xylene, toluene, chloroform, chlorobenzene, cyclohexanone] is presented. The structures were determined with microscopic techniques (atomic, AFM and lateral, LFM, force microscopy, fluorescent microscopy FM) and dynamic secondary ion mass spectrometry (dSIMS). The diagram, arranged according to the solubility parameter of the PTs and the solvents, exhibits three main structural classes: dewetting, lamellar, and lateral (quasi-2-dim) morphology. Decrease in PT solubility parameter δ_{PT} inhibits dewetting of polymer films. It induces also a transition from lamellar to lateral film structure. Increase in solvent solubility parameter δ_S has similar effects. Such behavior is related to the stability of transient homogeneous films and multilayers in the course of spin-casting. The role of δ_{PT} and δ_S is elucidated based on the stability analysis performed in terms of spreading coefficient (dependent on δ_{PT}) and effective interfacial tension of solvent-rich polymer phase (dependent on δ_S).

1. Introduction

The past decade has witnessed numerous efforts to apply solution-processed mixtures of conjugated polymers in low-cost, large-area electronics and optoelectronics.[1–6] Proposed main production strategies are based on additive polymer deposition to produce step-by-step all the functional elements of potential devices. Spin-casting of polymer blends is technologically more attractive as it offers a one-step process to demix, deposit and align simultaneously domains, rich in different polymers, which form various device elements: Self-stratified *lamellar* structures were used to produce (encapsulated[7]) field effect transistors FETs,[8] efficient light emitting diodes LEDs,[9] photovoltaic PV devices,[10,11] and bilayer conductors/insulators.[12,13] Also *lateral* film morphologies were applied to fabricate structured (insoluble[14]) films of (semi)conductors[15,16] and LEDs with voltage-controlled color.[17] In turn, bicontinuous fine morphologies were reported to increase quantum PV efficiency.[3] Finally, the substrate patterns were used to align *lateral* morphologies[18] and photonic structures optimizing LED performance[19] and to guide film structures on the submicrometer scale.[20,21]

Despite such successes in technological developments, much less has been done to examine systematically the effects of exact spin-casting conditions on film structure formation by conjugated polymer mixtures and to resolve its relevant mechanisms, which might differ from those for model polymers.[5,22] Only very recently have systematic works been reported, e.g., on polyfluorene/polyfluorene[2] and polyfluorene/fullerene blends.[22] Such studies are often difficult, as the quantitative physicochemical parameters important for solution processing are rarely available for novel conjugated polymers.

One of the most studied polymer families for (semi)conductor/optical applications are polythiophenes, in particular poly(3-alkylthiophenes) PTs or their derivatives. This is due to their superior charge mobility (up to 0.6 cm^2/Vs) and commercial availability.[23] Mixtures of insulating polymers with these high-performance semiconductors were often used to spin cast the structured films for diverse device designs:[7,14–16,20,21,24–28] *Lateral* blend morphologies were proposed to fabricate submicrometer size LEDs,[15] LEDs with varied color,[15] white light emitters,[16,28] and anisotropic (semi)conductor layers.[14,15] In turn, the *lamellar* structures were applied to produce PT-based FETs with a (self-stratified) protective[7] or (deposited) gas sensing[29] layer. In addition, blend multilayers could be *dewetted* locally, mimicking the chemical substrate patterns,[20,21] suggesting a novel route to produce plastic circuitries.

In this paper, we present the first systematic study on the film morphology of polythiophenes mixtures with a dielectric polymer. We focus on the structure formation of polystyrene PS blended with various poly(3-alkylthiophenes) PTs (regioregular R-P3DDT, R-P3HT, and regiorandom P3BT, P3DDT) and spin-cast from different common solvents (*p*-xylene, toluene, chloroform, chlorobenzene, cyclohexanone). This work is an extension of two of our previous studies: PT solubility parameters δ_{PT} (and negligible moisture absorption) were determined in ref 30. Impact of humidity and solvent volatility was examined in ref 31 for the PS/P3BT blends spin-cast from chloroform, cyclohexanone, and tetrahydrofuran (THF). It was shown that humidity effects can be avoided if the films are cast from the solvents that are less hygroscopic than THF.

The results of extended morphological studies are summarized here as a polymer vs solvent diagram of film structures, arranged according to the solubility of four PTs and five solvents. Analysis of this diagram reveals two morphological transitions from *dewetted* to continuous films, and from *lamellar* to *lateral* structures, which can be induced by a change of solubility parameter: decreased for PT polymers or increased for the solvents. This is a novel situation: lamellar-lateral transition was reported previously to be controlled by polymer solubility[32,33] and[22]/or[10] solvent evaporation rate.[10,22] A similar role of PT (decreased) and solvent (increased) cohesion energy density is related with an interface between PT-rich phase and PS-rich solution, which might be formed in the course of spin-casting

* Corresponding author. E-mail: ufbudkow@cyf-kr.edu.pl.
† Faculty of Physics and Applied Computer Science, AGH-University of Science and Technology.
‡ Department of Physics, Karlstad University.
§ M. Smoluchowski Institute of Physics, Jagiellonian University.

10.1021/ma7022974 CCC: $40.75
Published on Web 06/11/2008

Table 1. Solubility Parameters δ of Materials Used in This Study

material	δ/MPa$^{1/2}$	$[\delta - \delta(\mathrm{PS})]$/MPa$^{1/2}$
R-P3DDT	12.5 ± 0.2^a	−5.3
R-P3HT	13.1 ± 0.3^a	−4.7
P3BT	15.3 ± 0.4^a	−2.5
P3DDT	16.9 ± 0.8^a	−0.9
PS	17.8 ± 0.8^b	
p-xylene	18.0^b	0.2
toluene	18.2^b	0.4
chloroform	19.0^b	1.2
chlorobenzene	19.4^b	1.6
cyclohexanone	19.6^b	1.8

[a] Reference 30. [b] Reference 34.

to stabilize films against dewetting or/and to initiate lamellar-lateral transition.

2. Experimental Section

Preparation of Blend Films. Polymers used in this work were polystyrene (PS, glass transition point $T_g = 373$ K,[34] surface energy $\gamma = 40.7$ mJ m^{-2},[34] molecular weight $M_w = 65$K, polydispersity index $M_w/M_n = 1.02$), provided by Polymer Standard Service, Mainz, Germany, and four different poly(3-alkylthiophenes) (PTs, synthesized using the Rieke method[35]) purchased from Aldrich Chemical Co. Regiorandom poly(3-butylthiophene) (P3BT, $\gamma = 28.9 \pm 0.6$ mJ m^{-2} [30]) and poly(3-dodecylthiophene) (P3DDT, $T_g = 230$ K[36]) were both reported by the supplier to have a 1:1 ratio of HH:HT (head-to-head: head-to-tail) linkages. In turn, regioregular poly(3-hexylthiophene) (R-P3HT, melting point $T_m = 489$, 508 K,[37,38] $\gamma = 21.0 \pm 0.2$ mJ m^{-2},[30] $M_w \sim 87$K) and poly(3-dodecylthiophene) (R-P3DDT, $T_m = 448$ K,[39] $\gamma = 19.8 \pm 0.9$ mJ m^{-2},[30] $M_w \sim 162$K) were specified by HT regioregularity >98.5%.

The polymers were used as obtained to prepare symmetric (1:1 mass fractions of PS:PT) binary blends dissolved in analytic grade common solvents, with low ($\gamma \leq 28.0$ mJ m^{-2};[40] *p*-xylene, toluene, chloroform) and high surface tension ($\gamma \geq 33.0$ mJ m^{-2};[40] chlorobenzene, cyclohexanone), at constant concentration $c_P = 20$ mg/mL. Additional measurements were performed for asymmetric blends (4:1 w:w PS/PT) with lateral film morphology. Solubility parameters of pure solution components are listed in Table 1. Films were prepared from the blend solutions by spin-casting (3500 rpm for 30 s, with KW-4A apparatus, Chemat Technology) onto silicon wafers covered with a native oxide (SiO_x, with surface energy $\gamma = 36.5$ mJ m^{-2} [41]). The average film thickness, determined from AFM images taken after partial film removal,[42] ranged from 55 to 180 nm.

Blend Film Characterization. Topography and friction surface images (scan range up to 60 μm × 60 μm) of the spin-cast PS/PT films were collected in air at room temperature by atomic (AFM) and lateral (LFM) force microscopy (The Academia System, Nanonics Imaging Ltd., Israel) working in contact mode (control measurements were also performed in noncontact mode). LFM resolves surface domains rich in different polymers.[42] AFM and LFM data were used to confirm the correspondence between lateral domain structure (LFM) and film topography (AFM).[31] In addition, a procedure combining an examination by AFM with preferential PS dissolution (in cyclohexanone or hot dimethylformamide for the PS mixtures with regioregular or regiorandom PTs, respectively) was applied to verify overall blend film morphologies. The surface domains were identified unequivocally by fluorescence microscopy (FM) (Olympus Reflected Fluorescence System). FM images (imaged area up to 220 μm × 290 μm) of the domains rich in PT were obtained using a Hg illumination source and fluorescence mirror units Olympus U-MNB2 (excitation filter transmitting light at 470M–490 nm and a 520 nm low pass filter) or Olympus U-MNG2 (excitation filter at 530–550 nm and a 590 nm low pass filter) matching the PT absorption spectrum. Additional measurements were made with a Near-Field Scanning Optical Microscope (NSOM) (MultiView 1000, Nanonics Imaging Ltd., Israel) working in a fluorescence transmission mode.

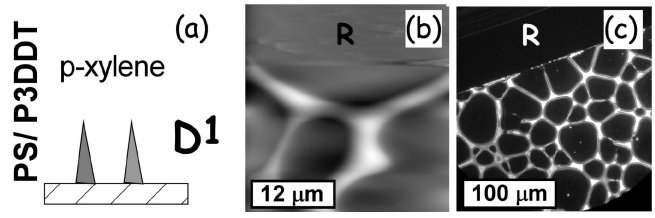

Figure 1. Schematic sectional view of the dewetted film morphology D^1 (a) concluded, based on AFM (b) and FM (c) images, for PS/P3DDT blend film cast from *p*-xylene. Regions with removed film (R) are marked in parts b and c. The fluorescence signal in part c corresponds to PT. The gray level depicts the height scale (b, height range $\Delta H = 120$ nm) or fluorescence intensity (c, white corresponds to high values). Note that in reality the vertical extent of the film structure presented in part a is a few times lower than its horizontal dimensions.

Vertical phase domain arrangement in the blend films was determined with the depth profiling (depth resolution of ~10 nm[43]) mode of dynamic Secondary Ion Mass Spectrometry (dSIMS).[11–13,18,22,43,44] The dSIMS data were obtained with a VSW apparatus equipped with a high-resolution ion gun (liquid metal, Fei Co.) and a Balzers quadrupole mass spectrometer. A primary Ga^+ ion beam (5 keV, 2 nA) was used to sputter the sample and to induce secondary ions, which yielded mass-resolved information for the depth profiles. Mass/charge ratio 32 (S^-) was used as a label for the PT. Sputtering rate values for PS/PT blend components were confirmed by the experiments performed for pure polymer films.

3. Results

3.1. Three Classes of Spin-Cast Blend Film Structures. The determined structures of spin-cast PS/PT blends can be arranged in three different groups with morphologies characteristic for dewetted films (D), layered films (L) or films with lateral (quasi-2-dim, 2) domain arrangement.

3.1.A. Dewetting Morphologies D (D^1, D^L). This morphological class (D) is represented by two observed specific structures of dewetted films: First, a network-like polygonal structure with long ribbons (D^1), typical for the late stage of film dewetting,[45,46] was recorded for PS/P3DDT blends spin-cast from *p*-xylene (Figure 1). The "cellular" structure is characterized by holes of equal height as that of region R where the polymer film was removed (Figure 1b). This suggests that ribbons are composed of the blend, identified by the fluorescent PT in FM image (Figure 1c).

Second, a loose dispersion of large (ca. 20 μm) coalescing holes (Figure 2b,c), characteristic for the intermediate stadium of dewetting,[45] was observed in bilayers D^L (Figure 2a) formed by PS/P3DDT blends cast from chlorobenzene. The vertical film structure was determined with dSIMS (Figure 2d): Carbon profile (C^-_2 ions, solid squares, left logarithmic scale) is nearly constant with depth while PT signal (S^- ions, open triangles, right linear scale) is maximal for a layer closest to the silicon wafer (Si^- ions, solid circles, left scale). Limited sputtering time-range of the region with high PT concentration is compensated by a sputtering rate, much higher for regiorandom PT than PS, resulting in the thickness of PT layer comparable to that of PS lamella (in accord with 1:1 w:w PS/PT composition). Ring-like rims were formed around the holes (Figure 2b) by the blend displaced from the hole areas as indicated by PT fluorescence micrograph (Figure 2c): the FM image clearly shows dewetted spots (black), PT-containing blend rims (light) and PT lamellae covered by a top PS layer (areas with lower FM intensity).

3.1.B. Lamellar Structures L (L^1, L^D). Lamellar structures (L) exhibited two specific morphologies: First, the bilayers (L^1) with continuous PS-rich upper and PT-rich bottom layer (Figure

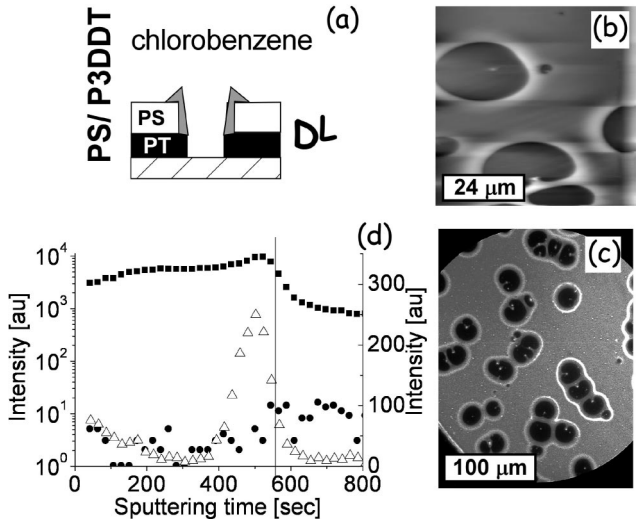

Figure 2. Schematic sectional view (a) of a dewetted film with lamellar morphology D^L (a) determined based on AFM (b, height range $\Delta H = 90$ nm), FM (c), and dSIMS (d) data for PS/P3DDT blend spin-cast from chlorobenzene. Depth dSIMS profiles in part d correspond to the total polymer composition (C_2^- ions, $m/z = 24$, solid squares, left logarithmic scale), the PT concentration (S^- ions, $m/z = 32$, open triangles, right linear scale) and Si ($m/z = 28$, solid circles, left scale). Sputtering time measures the distance from the original surface (1 s ~ 0.12 and 0.28 nm for PS and P3DDT, respectively).

3a) were observed in PS/P3BT blend films cast from chloroform.[31] This structure was also observed in other systems such as PS/P3DDT spin-coated from toluene or chloroform and PS/P3BT spin-cast from toluene.

Second, a similar bilayer structure L^D, but with dewetted upper PS lamella (Figure 3b), was observed for PS/P3BT films spin-cast from chlorobenzene. A lateral phase domain arrangement with elevated PS-rich and depressed PT-rich phases, both facing air, is concluded when AFM (Figure 3c) and FM (Figure 3d) images are compared. This information can be combined with dSIMS results to yield the overall structure of fragmented upper (PS-rich) phase immersed in lower (PT-rich) lamella (Figure 3b). Such a specific film morphology yields characteristic dSIMS profiles (Figure 3e), determined previously for other film mixtures[44,47] (with similar and different sputtering rates of blend components.[44,47,48]). The composition vs depth profiles (Figure 3e) of carbon (solid squares, left logarithmic scale), PT (open triangles, right linear scale), and Si (solid circles, left logarithmic scale) exhibit four consecutive periods of sputtering: Initially, a continuous undulated blend film with laterally arranged air-facing phases (rich in PT and PS) is present (see sketch I in Figure 3f) and the signals from all polymers (C_2^- ions) and PT (S^- ions) are maximal. Then the lower film regions occupied previously by PT are sputtered away (sketch II in Figure 3f), since the sputtering rate is higher for the phase rich in PT as compared to PS. As a result, the S^- yield is minimal and that of C_2^- ions reduced. Later on, all original PS-rich elevations are etched uncovering located beneath, and now unprotected, remaining regions of PT-rich lamella (sketch III in Figure 3f); hence, PT concentration is increased but carbon intensity unchanged. Finally, all the polymer material is sputtered away (sketch IV in Figure 3f), and the Si signal is saturated.

The dSIMS data of the vertical film structure (Figure 3e) match well, on a quantitative level, the microscopic data of horizontal surface morphology (Figure 3c): The ratio of C_2^- signal intensity $I_2/I_1 = 0.62(9)$, evaluated for the plateaus of two first sputtering periods (Figure 3e), accords well with the surface area fraction of elevated PS-rich regions $F = 0.58(1)$ determined from AFM (Figure 3c) with integral geometry approach[49] (see also Figure S1 of the Supporting Information). The ratio of PT surface areas exposed during the third (stage III) and the first (stage I) sputtering period is $F/(1 - F) = 1.4(6)$ (Figure 3f). This is the reason why the S^- yield is ~1.4 times larger during stage III as compared to the first period. The L^D structure of PS/P3BT films spin-cast from chlorobenzene (Figure 3b) was confirmed independently by the AFM images (see Figure S1) taken prior and after preferential dissolution (Figure S2) of the PS-rich phase.

The bilayers with perforated PS lamella were also observed in PS/P3BT and PS/R-P3HT blends spin-coated from *p*-xylene (see Figure S3 of the Supporting Information). However, the fraction of perforated surface is here much smaller than in L^D and the overall structure, reflected by dSIMS profiles, resembles the morphology L^1.

3.1.C. Lateral Morphologies 2 (2^T, 2^S). This morphological class (2) is characterized by lateral domain structure extending from the substrate through the PS/PT blend film to the surface. While the domain structure is always correlated with the film topography, the elevated domains are formed by the phase rich in PT or PS forming two specific morphologies, 2^T or 2^S, respectively (Figure 4, parts a and b). The first morphology (2^T) was recorded[31] for PS/P3BT films spin-cast from cyclohexanone.[31] It was also found for other systems such as PS/P3DDT spin-coated from cyclohexanone, PS/R-P3HT spin-cast from toluene or chloroform (Figure S4) and PS/R-P3DDT cast from chloroform.

The second specific structure (2^S, Figure 4b) was observed for PS/R-P3DDT blends spin-cast from chlorobenzene (Figure 4b−e). AFM (Figure 4c) and FM (Figure 4d) micrographs show lateral arrangement with elevated PS and depressed PT phases facing air. Both phases extend throughout the whole blend film (Figure 4b), as concluded based on characteristic dSIMS spectrum (Figure 4e), similarly to determined earlier for another blend with the same morphology.[44] The composition vs depth profiles exhibit three periods of polymer sputtering: First, both air-facing phases are present (see sketch I in Figure 4f); hence C_2^- (solid squares) and S^- (open triangles) signals are maximized. Later on, the depressed PT-rich phase is totally sputtered away exposing the SiO_x substrate (sketch II), since the PT-rich domains are thinner than the phase rich in PS. It results in an increase in the silicon yield (solid circles), a dip in the carbon intensity and a drastic reduction of the S^- signal. Finally, all the polymer material is etched (sketch III), and the Si intensity is saturated.

The lateral structure 2^S (Figure 4b) is confirmed by two following observations: First, the surface fraction of elevated (PS-rich) regions $F = 0.42(3)$, determined from AFM images (Figure 4c, see also Figure S5), agrees well with the ratio of carbon intensity (Figure 4e) evaluated for two first sputtering periods $I_2/I_1 = 0.45(4)$. Second, the micrographs taken prior and after the selective dissolution of the PS-rich phase (Figure S5) accords with the structure of Figure 4b.

The 2^S morphology was concluded also for PS/R-P3DDT blends spin-cast from *p*-xylene or toluene and for PS/R-P3HT films spin-coated from chlorobenzene (Figure S6).

3.2. Polymer vs Solvent Diagram of Blend Film Structures. The PS blends with R-P3HT and R-P3DDT could not be dissolved in cyclohexanone. All remaining blend−solvent systems resulted in 18 spin-cast films which morphologies can be consistently arranged (Figure 5) according to the solubility parameter of the PTs (δ_{PT}) increasing from R-P3DDT (bottom) to P3DDT (top),[30] and the solvents (δ_S) increasing from *p*-xylene (left) to cyclohexanonone (right)[34] (for δ values see Table 1 and Figure 6a). Representative AFM (white labels) and LFM (black labels) micrographs of all studied PS/PT blends are shown

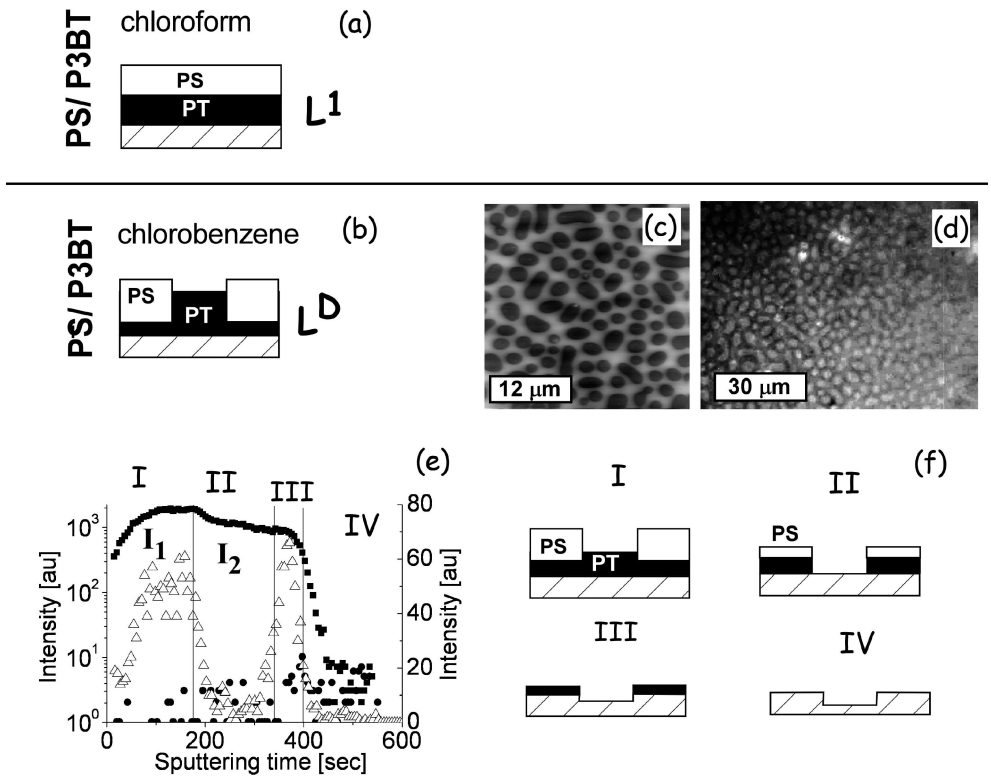

Figure 3. Schematic sectional views of lamellar morphology L^1 (a) and bilayer structure L^D with dewetted upper PS lamella (b) determined for PS/P3BT blend films cast from chloroform [31] and from chlorobenzene (this study), respectively. The structure L^D (b) is concluded based on AFM (c, height range $\Delta H = 15$ nm) and FM (d) images as well as dSIMS profiles (e). Sputtering time in part e measures the distance from the original nonplanar surface (1 s $\sim$ 0.17 and 0.32 nm for PS and P3BT, respectively). (f) Sketches to illustrate sectional views of phase domains exposed in consecutive sputtering periods.

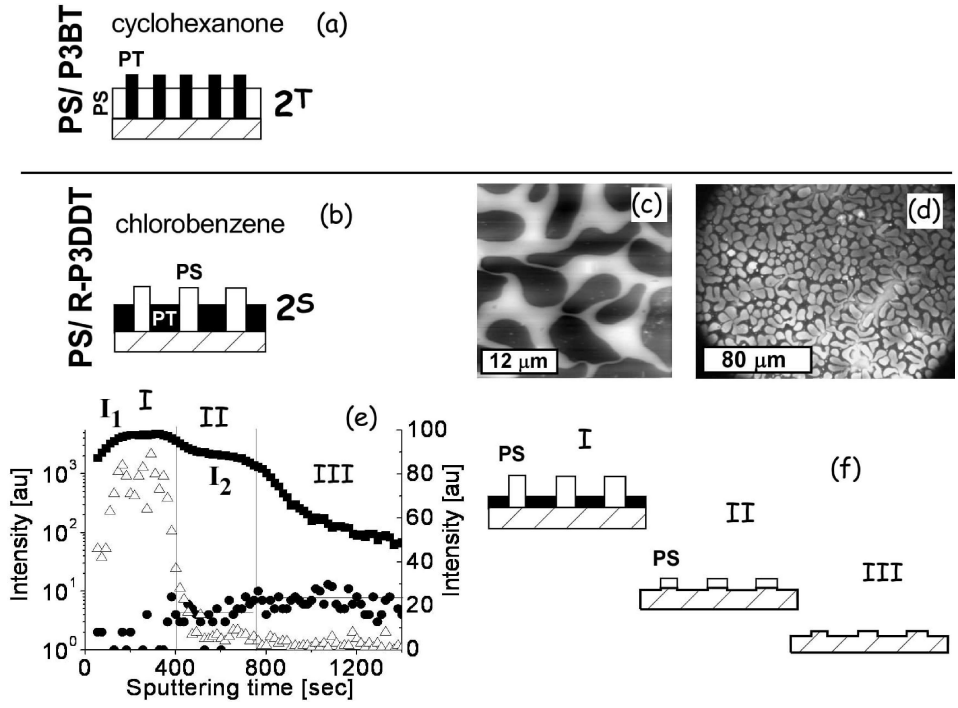

Figure 4. Schematic sectional views of lateral structures with elevated PT-rich phase 2^T (a) and elevated PS domains 2^S (b) determined for PS/P3BT cast from cyclohexanone [31] and PS/R-P3DDT from chlorobenzene (this study), respectively. The structure 2^S (b) is concluded based on AFM (c, height range $\Delta H = 50$ nm), FM (d), and dSIMS (e) data. Sputtering time in part e measures the distance from the original nonplanar surface (1 s $\sim$ 0.17 and 0.23 nm for PS and R-P3DDT, respectively). (f) Sketches to illustrate sectional views of phase domains exposed in consecutive sputtering periods.

in Figure 5. LFM images confirm lateral phase domain arrangement deduced from film topography.

The morphological data, illustrated in Figure 5, can be represented as a polymer vs solvent diagram of film structures.

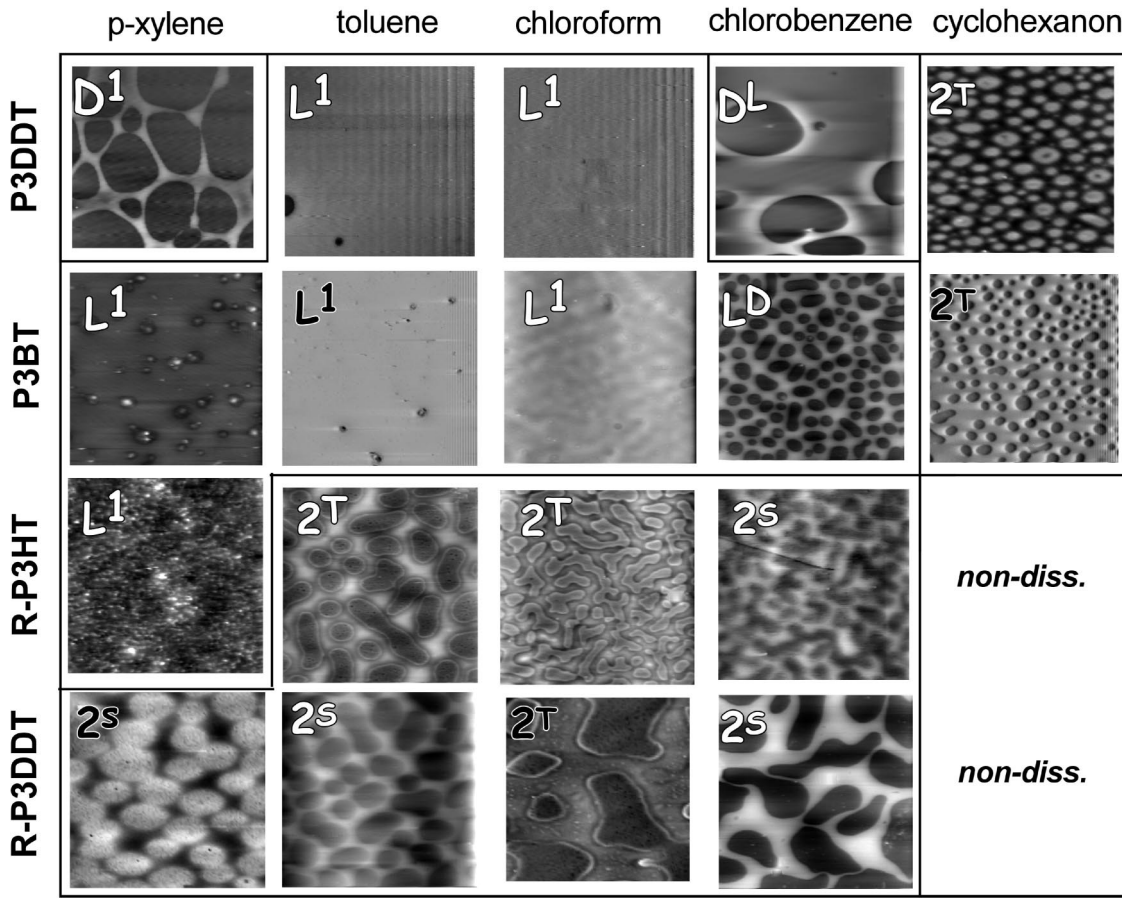

Figure 5. AFM (white labels) and LFM (black labels) images of PS/PT film blends spin-cast from common solvents, arranged according to the solubility parameter δ_{PT} of the poly(3-alkylthiophenes) (increasing from the bottom to the top[30]) and δ_S of the solvents (increasing from the left to the right[34]). Labels denote film morphology: dewetted D (D^1, D^L), lamellar L (L,[1] L^D) and lateral (quasi-2-dim) 2 (2^S, 2^T). Blends of regioregular PTs with PS could not be dissolved in cyclohexanone. Scan range used is 30 μm × 30 μm, except for D^1 (70 μm × 70 μm) and D^L (60 μm × 60 μm). Height range in all AFM images $\Delta H < 50$ nm, except for D^1 ($\Delta H = 120$ nm) and D^L ($\Delta H = 90$ nm).

Such diagram (Figure 6b), in which three main morphological classes (D, L, 2) are marked, is the main experimental result of this study. It enables to notice the impact of both polymer and solvent solubility: Decrease in δ_{PT} inhibits film dewetting and induces a transition from lamellar to lateral structure. Increase in δ_S has similar effects.

4. Discussion

4.1. Structure Formation Model. To explain the characteristic morphological features of the studied PS/PT systems (Figure 5), as a function of the polymers and solvents used, it is necessary to consider the film structure formation taking place during the spin-casting of polymer mixtures. This is a complex process,[21,22,31–33,42,44,47,50–63] with rapidly varied thermodynamic and kinetic parameters, leading often to long-lived metastable structures.[33,50,54] While its consecutive stages (Figure 7a,b,d,e) have been observed directly, their detailed driving mechanisms are not yet completely resolved.[55,56] Existing models of spin-coating[57,61] with lamellar[53,58] and lateral[47,50,54,56] phase separation, as well as of liquid dewetting[45,46,52,64–71] are combined here to describe the scenario for PS/PT films (Figure 7), extended later (sections 4.2 and 4.3) to explain the role of δ_{PT} and δ_S.

First, most of the polymer solution is spun off (Figure 7a,b) leaving a uniform fluid film with homogeneous polymer composition (P), whose thickness is being reduced due to radial liquid flow.[33,57] Second, the decreasing (due to evaporation) solvent concentration makes the liquid prone to dewetting D (Figure 7b,c), when its surface tension is increased above the critical surface tension which is numerically nearly equal to the substrate energy [$\gamma(SiO_x) = 36.5$ mJ/m^2].[72] Surface tension of blend solution is a monotonic function of its composition[73] and depends on surface energies of its components: evaporating solvent ($26.4 \leq \gamma(\text{solvent}) \leq 34.6$ mJ m^{-2}) and polymers ($\gamma(PS) = 40.7$ mJ m^{-2} and $\gamma(PT) < 36$ mJ m^{-2}).

Solvent extraction initiates also lamellar phase separation (Figure 7b,d). When dewetting can be neglected, a complete lamellar structure L is formed, driven by the lower solubility of the demixed PT-rich phase as compared to that rich in PS (see Figure 6a). PT is more quickly (but not completely) depleted from solution and deposited on the SiO_x substrate[31,53,58,59] as a PT-rich lamella covered by PS-rich solution. A reversed layer arrangement (SiO_x//PS/PT) is favored by lower PT surface tension and lower (except for PS/P3DDT) interfacial energy of PS facing SiO_x.[74] Therefore, energy minimization[75] may drive the next morphological transition (Figure 7d,e) from lamellar structure L (SiO_x//PT/PS) to lateral morphology 2 (see section 4.2 for details). While the exact mechanism is not known, it has been suggested that the bilayer structure is broken up by a Marangoni-like instability of polymer/polymer interface, initiated when film thickness decreases below a certain critical value.[55,56,76] Most probably, holes are formed in the upper PS-rich solution layer, which are then filled by the lower PT-rich liquid phase analogously to scenario deduced for other systems.[50]

The quasi-2-dim structure, formed in a continuous polymer film, can develop further during subsequent lateral phase coarsening.[50,62] Phase evolution is terminated (as a lateral 2,

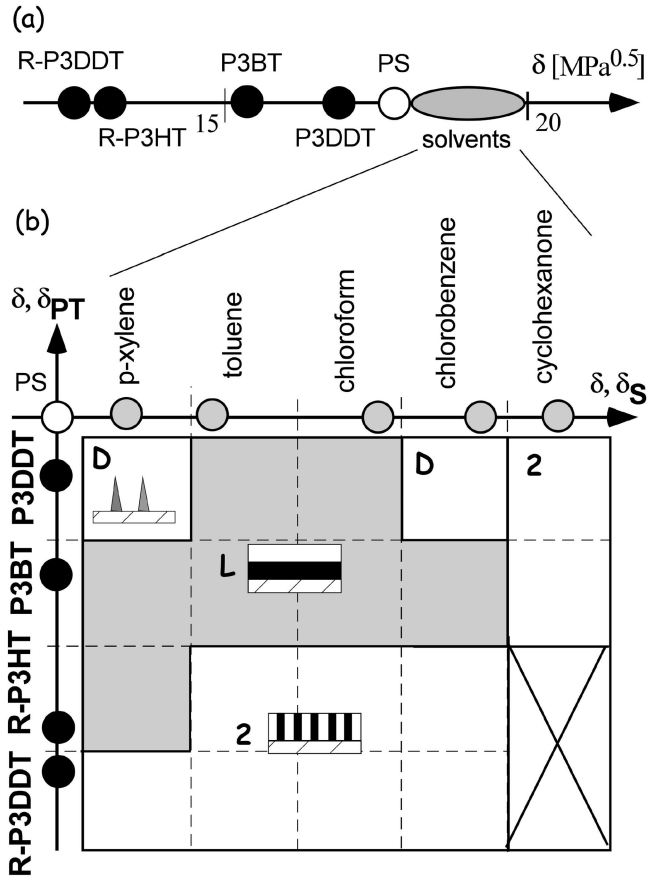

Figure 6. Polymer-solubility vs solvent-solubility relation (a) and a related diagram (b) of film structures revealed (Figure 5) in spin-cast PS/PT blends. The three main morphological classes (D, L, 2) are marked in the diagram.

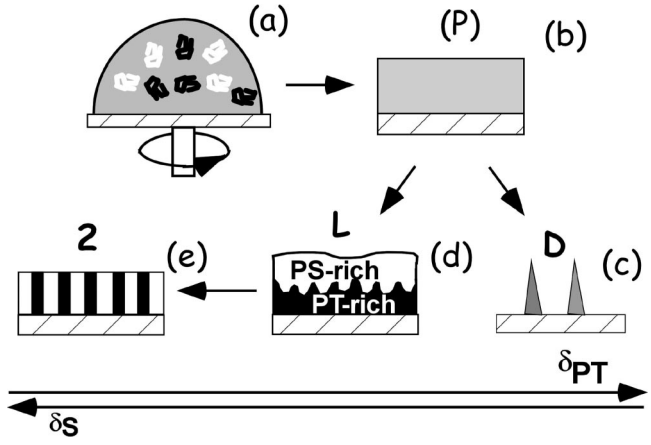

Figure 7. Model describing film structure formation in spin-cast PS/PT blends. The liquid film of homogeneous polymer solution (P) is prone to dewetting D or it evolves into a bilayer L (PT-rich lamella covered by PS-rich solution). The lamellar structure L can either be frozen in or be unstable resulting in lateral (quasi-2-dim) morphology 2.

lamellar L, or dewetting D structure), when solvent concentration is so low that the polymers are no longer mobile.[44,50]

Specific Morphologies. The above presented model of film structure formation in spin-cast PS/PT blends (Figure 7) is supported by the observed specific morphologies. For instance, the competing mechanisms of film dewetting (Figure 7b,c) and self-stratification (Figure 7b,d), acting on the liquid film of polymer solution (P), are reflected by the observed dewetted film with lamellar morphology D^L (Figure 2). In turn, an onset of morphological transformation from the lamellar to the lateral structure (Figure 7d,e) is "frozen" as a lamellar morphology with dewetted upper PS lamella L^D (Figure 3b−f). The perforations in the upper PS layer are filled completely by the PT phase in the lamellar structure L^1 with undulated interface, determined for PS/R-P3HT cast from *p*-xylene (Figure S3). Interfacial roughness present in the bilayers L^1 cast from chloroform[31] but not from other solvents with lower evaporation rate (Figure 3b−f) is a token of Marangoni instabilities driven by solvent gradients,[60,61] which can be removed by diffusion.[31,56,63]

For semicrystalline regioregular poly(3-alkylthiophenes), the formation of crystalline regions in amorphous phases is very limited during spin-casting,[38,77,78] especially for PTs with high molecular weight[78] (as used here), and therefore it has no impact on overall blend film structures (Figure 5). This situation corresponds to that recently observed for polyfluorene/fullerene blends cast in the fast film formation limit.[22]

For the blend films with lateral morphology 2, surface topography reflects domain structure (Figure 4 and Figures S4–S6). During the terminal stage of spin-casting the faster solidifying domains rich in PT (PS) form elevated regions of the structures $2^T(2^S)$ while the other phase collapses below this level to form depressed domains.[31] According to a simple model, fast inherent solvent desorption of PTs (higher than that of PS[30,31]) should lead to 2^T morphologies, as observed in PS/P3DDT and PS/P3BT blends cast from cyclohexanone, PS/R-P3HT mixtures spin-coated from two solvents (toluene and chloroform), and PS/R-P3DDT films coated from chloroform (Figure 5). However, the 2^S structures, observed for other systems, such as PS/R-P3HT blends coated from chlorobenzene and PS/R-P3DDT films spin-cast from three common solvents (*p*-xylene, toluene, chlorobenzene), suggest a more complex mechanism. It is possible that the limited formation of crystalline regions by regioregular molecules[77] (more mobile in the R-P3DDT- than in the R-P3HT-rich phase[38,39]) and the solvent-dependent difference in desorption times between PT and PS[31] is involved here.

4.2. Impact of Polymer Solubility on Blend Film Structures. There are two decisive moments during the film structure formation induced by solvent extraction (Figure 7): First, the destabilization of homogeneous polymer solution films (P) leads to dewetted film morphologies D (Figure 7b,c) while its absence - to continuous blend films (L or 2; Figure 7b,d,e). Second, the destabilization of transient bilayers results in lateral structure 2 (Figure 7d,e); alternatively the final structure is lamellar L. As relevant molecular forces are not all resolved, macroscopic Young's theory of contact angle phenomena[45,64–66,69] is used to perform stability analysis for homogeneous polymer solution *films* (P) and for individual *layers* PS and PT of the bilayer L.

The stability of a liquid film (2) on substrate phase (3) in the presence of fluid (gas or another liquid) (1) can be discussed in terms of the spreading coefficient[64,69,70]

$$S_{123} = \gamma_{13} - (\gamma_{12} + \gamma_{23}) \quad (1)$$

which measures the energy difference between the "bare" substrate exposed to the fluid (γ_{13}) and the substrate covered with a liquid film ($\gamma_{12} + \gamma_{23}$). If $S_{123} > 0$, the energy of the "bare" substrate is larger, hence the liquid will wet the substrate and the continuous liquid film will be stable (reaching at equilibrium complete wetting with $S_{123} = 0$). Alternatively ($S_{123} < 0$) the liquid film will create holes exposing the "bare" substrate (dewetting), and a finite contact angle for the liquid is formed (partial wetting).

To discuss the continuous-dewetted structure transition for a series of PT systems we have calculated (with eq 1) the

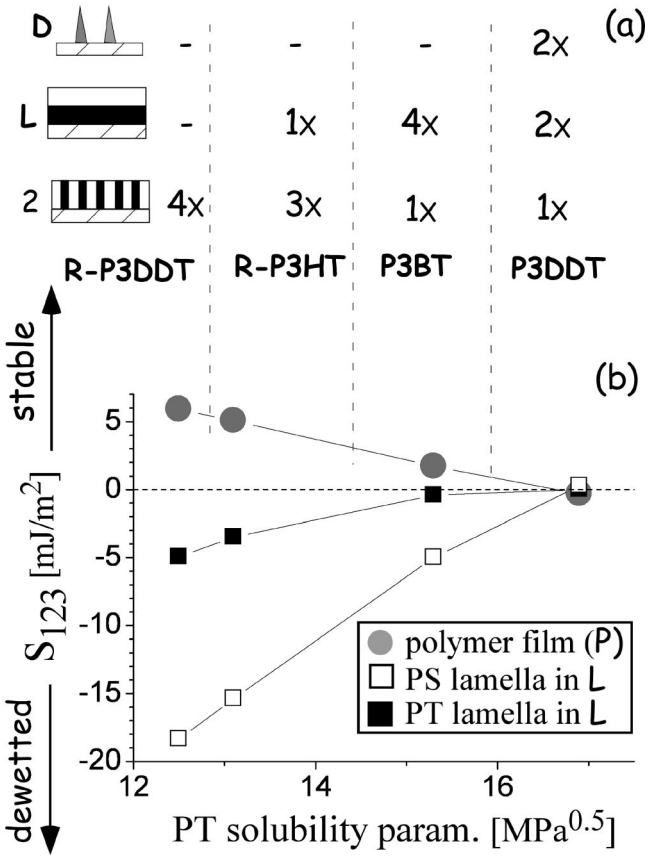

Figure 8. Frequency of various morphological classes observed for PS blends with different poly(3-alkylthiophenes) (a) compared with results of stability analysis (b) performed for a polymer solution monolayer (P) (gray circles) as well as for solvent-rich PS layer (open squares) and PT lamella (solid squares) of lamellar structure L.

spreading coefficient S_{123}[74] for the polymer solution film (P) on SiO_x substrate in the presence of air. The polymer solution (P) was represented by a surface energy γ averaged between that of PT, PS and a mean solvent value. To reflect lower solvent concentration, the weighted average of γ was used with weights 1, 1, and 0.5 assigned to PS, PT and solvent, respectively.

In turn, the lamellar-lateral transition in spin-cast PT blends is an analogue[22] of the wetting transition in annealed blends (1)/(2):[79,80] In both cases the liquid (2) wets, completely or partially, the confining surface (3) in the presence of another liquid (1). To analyze completely the stability of transient bilayer structures (SiO_x//PT/PS), the S_{123} values were calculated with eq 1[74] for both layers: (i) the PS-rich solution wetting free surface in the presence of PT; (ii) the PT-rich phase spreading on the SiO_x substrate with the PS-rich solution present. The surface tension of PT-rich phase was represented by that of pure PT while the value for the PS-rich solution was averaged between that of PS and the solvent.

The results of such (macroscopic) stability analysis are presented in Figure 8b as a function of PT solubility parameter δ_{PT}, modifying the polymer surface tension $\gamma \sim \delta_{PT}^2$.[30,81] We notice at once two characteristic features: First, with increasing δ_{PT} the spreading wetting of polymer solution film (P) is reduced (gray circles in Figure 8b) to reach a negative S_{123} value for P3DDT, whereas the bilayer lamellae become more stable (open and solid squares). Second, the absolute S_{123} values of PT layers are much smaller than those of solvent-rich PS lamellae in the bilayers L (except for P3DDT). These predictions are not changed, when the calculations are made for pure polymers (i.e., without solvent).

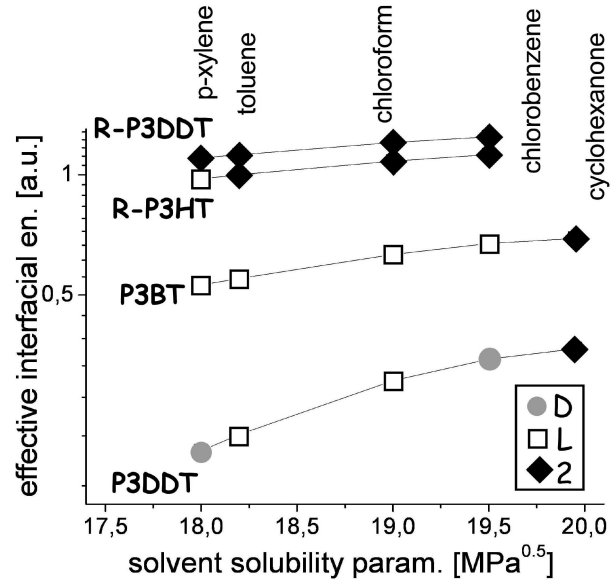

Figure 9. Effective interfacial energy between a solvent-rich PS phase (50% concentration) and various poly(3-alkylthiophenes) PTs as a function of the solvent solubility parameter δ_S. Corresponding morphologies of PS/PT films are marked by different symbols (D, gray circles; L, open squares; 2, solid diamonds).

Both features of Figure 8b are well reproduced by the spin-cast PS/PT blends: First, dewetted film morphologies are manifested only for P3DDT (with the highest δ_{PT}), while the frequency of lateral structures 2 (resulting from bilayer destabilization) decreases with increasing PT solubility from R-P3DDT to P3DDT (Figure 8a). Second, only specific morphologies reflecting the destabilized PS lamellae (Figures 3b−f and S3) but not PT layers are observed in spin-cast blends (PS/P3BT and PS/R-P3HT).

A careful analysis of Figure 8b reveals another interesting feature. Not only the spreading parameter of the polymer solution (P), but also those of both transient layers (PS-rich solution and PT-rich phase) change their sign for P3DDT. This specific result, described by the relations $S_{123}(PT) > 0$, $S_{123}(PS) > 0$, and $S_{123}(P) < 0$, indicate that (transient) bilayers of the phase separated (P3DDT/PS) films are stable while homogeneous polymer solution films dewet the substrate. This leads us to the conclusion that phase separation could inhibit film dewetting in the course of blend spin-casting.

4.3. Impact of Solvent Solubility on Blend Film Structures. Thermodynamic phase diagram of the ternary system A/B/S of two molecules A and B in a common solvent S is determined mainly by the interactions between both molecules while the solvent interactions play negligible role.[22] To understand the impact of the solvent on phase separation and final blend structures, the film structure formation model (section 4.1) must be recalled: The phase evolution in the spin-cast films is driven by the interface formed between PT-rich phase, considerably depleted of solvent, and PS-rich solution. This resembles model interface formed between a homopolymer (PT) and random copolymer ($PS_{1-x}S_x$).[82] This analogy can be used to approximate effective interfacial tension by[83]

$$\gamma_{PT,PS}^{eff} \sim [x\chi_{PT,S} + (1-x)\chi_{PT,PS} - x(1-x)\chi_{PS,S}]^{1/2} \qquad (2)$$

Using interaction parameters χ_{ij} approximated by solubility parameters $\chi_{ij} \sim (\delta_i - \delta_j)^2$, we have evaluated with eq 2 the effective energy of the interface between PT and the PS-rich solution (Figure 9). We notice that interfacial tension between these transient phases depends on solvent solubility δ_S. The strongest dependence is predicted for P3DDT while the weakest

for regioregular PT polymers. This can be related with large and small solvent impact on the structure formation in P3DDT and R-P3DDT blends, respectively (Figure 6).

Stability analysis performed for the P3DDT/PS system (the last result of section 4.2) shows phase-separated films to be more stable against dewetting than those with homogeneous composition. For the same system, increasing solvent solubility δ_S induces considerable rise of effective interfacial energy (Figure 9) interpreted as an increased tendency for demixing and phase evolution. Therefore we expect film dewetting to be inhibited for P3DDT/PS cast from solvents with higher δ_S. This is in fact observed (Figure 6) for two solvent classes: with low ($\gamma_S \leq 28$ mJ/m^2; *p*-xylene, toluene, chloroform[40]) and high ($\gamma_S \geq 33$ mJ/m^2; chlorobenzene, cyclohexanone[40]) surface tension: The dewetting visible for *p*-xylene is stopped for toluene and chloroform (higher δ_S). It reappears, manifested as dewetted lamella D^L, for chlorobenzene (high γ_S), and is inhibited again due to increased δ_S for cyclohexanone. To our knowledge, this is first observation of phase separation that inhibits dewetting during the spin-casting process. Analogous behavior was observed earlier only for thermally annealed films.[84–87]

An increase in solvent parameter δ_S, giving a larger effective interfacial tension γ_{23} (Figure 9), would also result in the reduced value of the spreading coefficient S_{123} (see eq 1) for both lamellae (PS-rich solution and PT-rich phase) in a transient bilayer L. As a consequence morphological transition from lamellar L to lateral 2 morphology should be favored. This is indeed observed for P3DDT, P3BT and R-P3HT blends (Figures 5 and 6) when the solvents with higher δ_S are used.

5. Summary and Conclusions

To summarize, we present the first systematic morphological study on the spin-cast blends of poly(alkylthiophenes) PTs—high-performance semiconductors, mixed with a dielectric polymer—polystyrene PS. The polymer vs solvent diagram of film structures, formed in the spin-cast PS/PT blends, is arranged according to the solvent- and PT-solubility parameters δ. Visible control of final film morphology (dewetted, lamellar or lateral) is related to the stability of transient layers: homogeneous films and demixed multilayers formed in the course of solution processing and dependent on surface energy $\gamma \sim \delta^2$. Results of stability analysis performed for transient films and multilayers correlate well with the observed impact of polymer (δ_{PT})- and solvent (δ_S)-solubility on blend film structure. Both, δ_{PT}- and δ_S-effects are similar and related with an interface between the PT-rich phase and the PS-rich solution, which stabilizes films against dewetting or/and initiates the lamellar−lateral transition.

Dewetting of blend films is successfully inhibited by solubility parameter: decreased for PT or increased for solvent. Phase separation plays an important role in the latter effect. Mixtures inhibiting dewetting have been observed so far only for thermally annealed films.[84–87]

Components of spin-casting solution control the morphological transition from lamellar to lateral structures. The latter are favored when cohesion energy density is high for solvent and low for PT. They are formed from destabilized transient multilayers, evidenced earlier.[20,21]

This study was motivated by the idea of spin-casting semiconducting and insulating polymers as a one-step process to produce film morphologies highly relevant for applications, such as (opto)electronics. Film structure depends on the exact spin-casting conditions, such as blend composition, solvent solubility and volatility, ambient atmosphere and humidity, as well as substrate treatment. This work, together with an earlier publication,[31] discusses all these factors except for the last one, which is the issue of the current research. However, to increase charge-carrier transport in the potential devices it might be necessary to subject the spin-cast blends to post-treatments, such as thermal,[88] electrical,[89] or solvent[90] annealing. This should enhance formation of PT crystalline regions and textures,[23] which is very limited during spin-casting[38,77,78] and hence without any impact on the overall morphology of the spin-cast PT/PS blends.

Acknowledgment. This work was partially supported by the Polish Committee for Scientific Research (Contract Grant No. 3 T08C 032 27), the European Community (under the Marie Curie Host Fellowships for the Transfer of Knowledge, project NEED), and the Reserve of the Faculty of Physics, Astronomy and Applied Computer Science of the Jagiellonian University.

Supporting Information Available: Figures showing the data used to determine the film structures of PS/R-P3HT blends spin-cast from *p*-xylene (Figure S3), chloroform (Figure S4), and chlorobenzene (Figure S6) and that used to confirm the film morphologies of PS/P3BT (Figure S1 and S2) and PS/R-P3DDT (Figure S5), both spin-cast from chlorobenzene. This material is available free of charge via the Internet at http://pubs.acs.org.

References and Notes

(1) Moons, E. *J. Phys.: Condens. Matter* **2002**, *14*, 12235.
(2) Arias, A. C. *J. Macromol. Sci., Polym. Rev.* **2006**, *46*, 103.
(3) Hoppe, H.; Sariciftici, N. S. *J. Mater. Chem.* **2006**, *16*, 45.
(4) Richards, D.; Cacialli, F. *Philos. Trans. R. Soc. London, Ser. A* **2004**, *362*, 771.
(5) Geoghegan, M.; Krausch, G. *Prog. Polym. Sci.* **2003**, *28*, 261.
(6) Reuss, R. H.; Hopper, D. G.; Park, J.-G. *MRS Bull.* **2006**, *6*, 447.
(7) Arias, A. C.; Endicott, F.; Street, R. A. *Adv. Mater.* **2006**, *18*, 2900.
(8) Chua, L.-L.; Ho, P. K. H.; Sirringhaus, H.; Friend, R. H. *Adv. Mater.* **2004**, *16*, 1609.
(9) Corcoran, N.; Arias, A. C.; Kim, J. S.; MacKenzie, J. D.; Friend, R. H. *Appl. Phys. Lett.* **2003**, *82*, 299.
(10) Arias, A. C.; Corcoran, N.; Banach, M.; MacKenzie, J. D.; Huck, W. T. S. *Appl. Phys. Lett.* **2002**, *80*, 1695.
(11) Björström, C. M.; Bernasik, A.; Rysz, J.; Budkowski, A.; Nilsson, S.; Svensson, M.; Andersson, M. R.; Magnusson, K. O; Moons, E. *J. Phys.: Condens. Matter* **2005**, *17*, L529.
(12) Bernasik, A.; Włodarczyk-Miskiewicz, J.; Łuzny, W.; Kowalski, K.; Raczkowska, J.; Rysz, J.; Budkowski, A. *Synth. Met.* **2004**, *144*, 253.
(13) Bernasik, A.; Haberko, J.; Wlodarczyk-Miskiewicz, J.; Raczkowska, J.; Luzny, W; Budkowski, A.; Kowalski, K.; Rysz, J. *Synth. Met.* **2005**, *155*, 516.
(14) Han, X.; Chen, X.; Holdcroft, S. *Adv. Mater.* **2007**, *19*, 1697.
(15) Grandström, M.; Berggren, M.; Pede, D.; Inganäs, O.; Andersson, M. R.; Hjertberg, T.; Wennerström, O. *Supramol. Sci.* **1997**, *4*, 27.
(16) Grandström, M.; Berggren, M.; Inganäs, O.; Andersson, M. R.; Hjertberg, T.; Wennerström, O. *Synth. Met.* **1997**, *85*, 1193.
(17) Berggren, M.; Inganäs, O.; Gustafsson, G.; Rasmusson, J.; Andersson, M. R.; Hjertberg, T.; Wennerström, O. *Nature* **1994**, *372*, 444.
(18) Haberko, J.; Raczkowska, J.; Bernasik, A.; Rysz, J.; Budkowski, A.; Łuy, W. *Synth. Met.* **2007**, *157*, 935.
(19) Fichet, G.; Corcoran, N.; Ho, P. K. H.; Arias, A. C.; MacKenzie, J. D.; Huck, W. T. S.; Friend, R. H *Adv. Mater.* **2004**, *16*, 1908.
(20) Coffey, D. C.; Ginger, D. S. *J. Am. Chem. Soc.* **2005**, *127*, 4564.
(21) Wei, J. H.; Coffey, D. C.; Ginger, D. S. *J. Phys. Chem. B* **2006**, *110*, 24324.
(22) Nillson, S.; Bernasik, A.; Budkowski, A.; Moons, E. *Macromolecules* **2007**, *40*, 8291.
(23) Salleo, A. *Mater. Today* **2007**, *10*, 38.
(24) Huang, Y.-J.; Hsieh, T.-H.; Wang, Y.-Z.; Chuang, C.-N.; Chen, Y.-P.; Huang, P.-T.; Ho, K.-S. *J. Appl. Polym. Sci.* **2007**, *104*, 773.
(25) Kanemoto, K.; Shishido, M.; Sudo, T.; Akai, I.; Hashimoto, H.; Karasawa, T. *Chem. Phys. Lett.* **2005**, *402*, 549.
(26) Masegosa, R. M.; Nava, D.; Garcia, S.; Prolongo, M. G.; Salom, C. *Thermochim. Acta* **2002**, *385*, 85.
(27) Monedero, M. A.; Luengo, G. S.; Moreno, S.; Ortega, F.; Rubio, R. G.; Prolongo, M. G.; Masegosa, R. M. *Polymer* **1999**, *40*, 5833.
(28) Grandström, M.; Inganäs, O. *Appl. Phys. Lett.* **1996**, *68*, 147.
(29) Sandberg, H. G. O.; Bäcklund, T. G.; Österbacka, R.; Jussila, S.; Mäkelä, T.; Stubb, H. *Synth. Met.* **2005**, *155*, 662.
(30) Jaczewska, J.; Raptis, I.; Budkowski, A.; Goustouridis, D.; Raczkowska, J.; Sanopoulou, M.; Pamuła, E.; Bernasik, A.; Rysz, J. *Synth. Met.* **2007**, *157*, 726.
(31) Jaczewska, J.; Budkowski, A.; Bernasik, A.; Raptis, I.; Raczkowska, J.; Goustouridis, D.; Rysz, J.; Sanopoulou, J. *Appl. Polym. Sci.* **2007**, *105*, 67.

(32) Affrossman, S.; O'Neill, M.; Stamm, *Macromolecules* **1998**, *31*, 6280.
(33) Gutmann, J. S.; Müller-Buschbaum, P.; Stamm, M. *Faraday Discuss.* **1999**, *112*, 258.
(34) Brandrup, I., Immergut, E. H., Grulke, E. A., Eds.; *Polymer Handbook*, 4th ed.; John Wiley & Sons: New York, 1999.
(35) Chen, T. A.; Wu, X.; Rieke, R. D. *J. Am. Chem. Soc.* **1995**, *117*, 233.
(36) Čik, G.; Šeršeň, F.; Dlhaň, L. *Synth. Met.* **2004**, *144*, 55.
(37) Yang, H.; Shin, T. J.; Yang, L.; Cho, K.; Ryu, C. Y.; Bao, Z. *Adv. Funct. Mat.* **2005**, *15*, 671.
(38) Park, Y. D.; Kim, D. H.; Jang, Y.; Cho, J. H.; Hwang, M.; Lee, H. S.; Lim, J. A.; Cho, K. *Org. Electron.* **2006**, *7*, 514.
(39) Causin, V.; Marega, C.; Marigo, A.; Valentini, L.; Kenny, J. M. *Macromolecules* **2005**, *38*, 409.
(40) Jasper, J. J. *J. Phys. Chem. Ref. Data* **1972**, *1*, 841.
(41) Zhao, W.; Rafailovich, M. H.; Sokolo, J.; Fetters, L. J.; Plano, R.; Sanyal, M. K.; Sinha, S. K.; Sauer, B. B. *Phys. Rev. Lett.* **1993**, *70*, 1453.
(42) Cyganik, P.; Budkowski, A.; Raczkowska, J.; Postawa, Z. *Surf. Sci.* **2002**, *507–510*, 700.
(43) Bernasik, A.; Rysz, J.; Budkowski, A.; Kowalski, K.; Camra, J.; Jedlinski, J. *Macromol. Rapid Commun.* **2001**, *22*, 829.
(44) Raczkowska, J.; Bernasik, A.; Budkowski, A.; Sajewicz, K.; Penc, B.; Lekki, J.; Lekka, M.; Rysz, J.; Kowalski, K.; Czuba, P. *Macromolecules* **2004**, *37*, 7308.
(45) Sharma, A.; Reiter, G. *J. Colloid Interface Sci.* **1996**, *178*, 383.
(46) Müller-Buschbaum, P. J. *Phys.: Condens. Matter* **2003**, *15*, R1549.
(47) Budkowski, A.; Bernasik, A.; Cyganik, P.; Raczkowska, J.; Penc, B.; Bergues, B.; Kowalski, K.; Rysz, J.; Janik, J. *Macromolecules* **2003**, *36*, 4060.
(48) Raczkowska, J.; Bernasik, A.; Budkowski, A.; Rysz, J.; Kowalski, K.; Lekka, M.; Czuba, P.; Lekki, J. *Thin Solid Films* **2005**, *476*, 358.
(49) Raczkowska, J.; Rysz, J.; Budkowski, A.; Lekki, J.; Lekka, M.; Bernasik, A.; Kowalski, K.; Czuba, P. *Macromolecules* **2003**, *36*, 2419.
(50) Walheim, S.; Böltau, M.; Mlynek, J.; Krausch, G.; Steiner, U. *Macromolecules* **1997**, *30*, 4995.
(51) Müller-Buschbaum, P.; Gutmann, J. S.; Stamm, M. *Macromolecules* **2000**, *33*, 4886.
(52) Müller-Buschbaum, P.; Bauer, E.; Wunnicke, O.; Stamm, M. *J. Phys.: Condens. Matter* **2005**, *17*, S363.
(53) Ton-That, C.; Shard, A. G.; Teare, D. O. H.; Bradley, R. H. *Polymer* **2002**, *43*, 4973.
(54) Sprenger, M.; Walheim, S.; Budkowski, A.; Steiner, U. *Interface Sci.* **2003**, *11*, 225.
(55) Jukes, P. C.; Heriot, S. Y.; Sharp, J. S.; Jones, R. A. L. *Macromolecules* **2005**, *38*, 2030.
(56) Heriot, S. Y.; Jones, R. A. L. *Nat. Mater.* **2005**, *4*, 782.
(57) Lawrence, C. J. *Phys. Fluids* **1998**, *31*, 2786.
(58) Ton-That, C.; Shard, A. G.; Teare, D. O. H.; Bradley, R. H. *Polymer* **2001**, *42*, 1121.
(59) Schmidt, J. J.; Gardella, J. A.; Salvati, L. *Macromolecules* **1989**, *22*, 4489.
(60) Mitov, Z.; Kumacheva, E. *Phys. Rev. Lett.* **1998**, *81*, 3427.
(61) de Gennes, P. G. *Eur. Phys. J. E* **2001**, *6*, 421.
(62) Dalnoki-Veress, K.; Dalnoki-Veress, K.; Forrest, J. A.; Stevens, J. R.; Dutcher, J. R. *J. Polym. Sci., Part B: Polym. Phys.* **1996**, *34*, 3017.
(63) Müller-Buschbaum, P.; Gutmann, J. S.; Wolkenhauer, M.; Kraus, J.; Stamm, M.; Smilgies, D.; Petry, W. *Macromolecules* **2001**, *34*, 1369.
(64) Brochard-Wyart, F.; Daillant, J. *Can. J. Phys.* **1990**, *68*, 1084.
(65) Brochard-Wyart, F.; Martin, P.; Redon, C. *Langmuir* **1993**, *9*, 3682.
(66) David, M. O.; Reiter, G.; Sitthai, T.; Schultz, J. *Langmuir* **1998**, *14*, 5667.
(67) Chattopadhyay, S.; Meredith, J. C. *Meas. Sci. Technol.* **2005**, *16*, 128.
(68) Chattopadhyay, S.; Meredith, J. C. *Macromol. Rapid Commun.* **2004**, *25*, 275.
(69) de Gennes, P. G. *Rev. Mod. Phys.* **1985**, *57*, 827.
(70) Oslanec, R.; Costa, A. C.; Composto, R. J.; Vlcek, P. *Macromolecules* **2000**, *33*, 5505.
(71) Morariu, M. D.; Schäffer, E.; Steiner, U. *Phys. Rev. Lett.* **2004**, *92*, 156102–1.
(72) Van Krevelen, D. W. *Properties of Polymers: Their Correlation with Chemical Structure*; Elsevier: New York, 1976.
(73) Escobedo, J.; Mansoori, G. A. *AlChE J.* **1998**, *44*, 2324.
(74) For substances without hydrogen bonds, the interfacial energy $\gamma_{ij} \approx (\gamma_i^{0.5} - \gamma_j^{0.5})^2$, where γ_i and γ_j are surface tensions of the ith substance.[72]
(75) The conditions $\gamma_{PT,air} < \gamma_{PS,air}$ and $\gamma_{PS,SiO_x} < \gamma_{PT,SiO_x}$ lead to negative spreading coefficients for PS at air interface $S_{PT,PS,air} = \gamma_{PT,air} - (\gamma_{PT,PS} + \gamma_{PS,air})$ and for PT at SiO_x substrate $S_{PS,PT,SiO_x} = \gamma_{PS,SiO_x} - (\gamma_{PS,PT} + \gamma_{PT,SiO_x})$.
(76) The onset of the interfacial instability driven by van der Waals forces could occur only in films thinner than ~10 nm.[71]
(77) Hugger, S.; Thomann, R.; Heinzel, T. *Thurn-Albrecht, Colloid Polym. Sci.* **2004**, *282*, 932.
(78) Verilhac, J.-M.; LeBlevennec, G.; Djurado, D.; Rieutord, F.; Chouiki, M.; Travers, J.-P.; Pron, A. *Synth. Met.* **2006**, *156*, 815.
(79) Rysz, J.; Budkowski, A.; Bernasik, A.; Klein, J.; Kowalski, K.; Jedliński, J.; Fetters, L. J *Europhys. Lett.* **2000**, *50*, 35.
(80) Geoghegan, M.; Ermer, H.; Jüngst, G.; Krausch, G.; Brenn, R. *Phys. Rev. E* **2000**, *6*, 2–940.
(81) Koenhen, D. M.; Smolders, C. A. *J. Appl. Polym. Sci.* **1975**, *19*, 1163.
(82) ten Brinke, G.; Karasz, F. E.; MacKnight, W. J. *Macromolecules* **1983**, *16*, 1827.
(83) Helfand, E.; Tagami, Y. *J. Chem. Phys.* **1972**, *56*, 3592.
(84) Yerushalmi-Rozen, R.; Klein, J. *Langmuir* **1995**, *11*, 2806.
(85) Orlicki, J. A.; Moore, J. S.; Sendijarevic, I.; MacHugh, A. J. *Langmuir* **2002**, *18*, 9985.
(86) Mackay, M. E.; Hong, Y.; Jeong, M.; Hong, S.; Russell, T. P.; Hawker, C. J.; Vestberg, R.; Douglas, J. F. *Langmuir* **2002**, *18*, 1877.
(87) Li, X.; Han, Y.; An, L. *Polymer* **2003**, *44*, 5833.
(88) Nguyen, L. H.; Hoppe, H; Erb, T.; Günes, S.; Gobsch, G.; Sariciftci, N. S. *Adv. Funct. Mater.* **2007**, *17*, 1071.
(89) Padinger, F.; Rittberger, R. S.; Sariciftci, N. S. *Adv. Funct. Mater.* **2003**, *13*, 85.
(90) Li, G.; Yao, Y.; Yang, H; Shrotriya, V.; Yang, G.; Yang, Y. *Adv. Funct. Mater.* **2007**, *17*, 1636.

MA7022974